



SENSITIVITY OF OFFSHORE WIND TURBINE SEISMIC RESPONSE TO ROTOR MODELLING SIMPLIFICATIONS

A. Ali⁽¹⁾, R. De Risi⁽²⁾, A. Sextos⁽³⁾

⁽¹⁾ Ph.D. Student, Department of Civil Engineering, University of Bristol, UK, ahmer.ali@bristol.ac.uk

⁽²⁾ Lecturer, Department of Civil Engineering, University of Bristol, UK, raffaele.derisi@bristol.ac.uk

⁽³⁾ Professor, Department of Civil Engineering, University of Bristol, UK, a.sextos@bristol.ac.uk

Abstract

The rotor-nacelle-assembly (RNA) is an integral part of wind turbines, and it may contribute significantly to their total system mass. Notwithstanding its importance, it is a general practice to simplify the RNA as a concentrated mass in the structural response analysis of wind turbines. The rotor eccentricity and the rotary inertia of blades are two key structural parameters of a typical RNA. The first is often considered in the seismic performance assessment of wind turbines, however, the effect of the rotary inertia of blades is typically neglected. It is yet unknown how the dual consideration of these two parameters can influence the structural response and subsequently, the seismic vulnerability of wind turbines. This study investigates the combined effect of the two RNA parameters on the tower damage modes and failure probabilities of offshore wind turbines (OWT) under ground excitation due to shallow crustal earthquakes. Four different pairs of rotor eccentricity and rotary inertia of the blades are used. The modal analysis shows that the higher modes are affected by the inclusion of these two parameters. Interestingly, the non-linear dynamic analysis reveals the shift of the damage onset towards the upper and slenderer part of the tower. The fragility analysis further highlights the significant uncertainty associated with the measured failure probabilities of the OWT tower. The probability of failure is considerably lower if the rotary inertia and rotor eccentricity are ignored which demonstrates that the common modelling simplifications can potentially lead to unconservative design.

Keywords: Renewable energy; Seismic design; Offshore wind turbines; Tower failure; Failure probability

1. Introduction

In a probabilistic seismic risk assessment (PSRA) framework, structural analysis is vital to evaluate the response of a structure to various intensities of a characteristic earthquake hazard. It involves the development of a numerical model that facilitates the preliminary analysis of the nonlinear dynamic behavior of the structure. The modeling complexity can range from a simple 1-dimensional (1D) beam element model [1,2] to a high-fidelity 3D finite element model (FEM) [3,4]. The choice of the model complexity depends on the desired computational efficiency and the nature of the required structural response. For instance, the simple 1D beam elements are efficient for simulating the global structural response [5] whereas the detailed 3D FEM is suitable for identifying local failure mechanisms of a structural component [6–8].

Regardless, the reliability of the structural response depends on how rigorously the uncertainties in structural parameters that define the computational model are considered [9]. Such parameters may include mass, stiffness, damping, strength, boundary conditions, among others. Generally, the ground motion variability is considered more significant in affecting the structural response or the engineering demand parameters (EDP) in a PSRA [10], therefore, structural parameters are often simplified to reduce the computational effort. In the case of wind turbines, the rotor-nacelle-assembly (RNA) at the tower top is often idealized as a point mass [2,5–8,11]. This is done because the RNA details, such as the rotor diameter, and the mass of the nacelle, hub, and the blades are easy to find. On the contrary, it is often difficult to acquire the local details of the blades, including their shape profile, material distribution and strength. This hinders the accurate modelling of the blade models into the global FEM of a wind turbine. Hence, the lumped mass idealization of the RNA serves as the common and a time-efficient choice, particularly, when the non-linear

structural analysis involves a large number of seismic time histories [2,6,11] even though this approach is unable to capture the influence of local blade modes and the effects of their modal damping on the global system response.

It is important to note that the nacelle and the rotor (hub and the blades combined) of a typical RNA are horizontally and vertically-eccentric to the tower. The nacelle constitutes a major portion of the total RNA mass (M_{RNA}) which can nearly be equal to half of the total wind turbine's mass [12]. M_{RNA} is shown to be one of the key parameters in determining the tower failure in offshore wind turbines (OWT) under crustal earthquakes [5]. Moreover, the blades are long and slender structures that tend to induce rotary inertia effects at the tower, which can be generically considered into the structural analysis if the blades are modeled explicitly [3]. However, in the case of the lumped mass approach, this feature needs to be invoked into the idealized system using analytical computations [2]. Within the context of the simplified RNA, the literature shows a mixed practice for the mutual consideration of the two RNA parameters, i.e. (i) rotary inertia of the blades, and (ii) the rotor/RNA eccentricity. Only a limited number of studies have considered the rotary inertia effects in conjunction with the rotor eccentricity, taken as either only vertical [2,5] or in both horizontal and vertical directions [7,8,13]. Moreover, so far, it remains unclear how the interaction of the two aforementioned parameters would impact the structural response of wind turbines under transient seismic loading.

Along these lines, this study aims at addressing the above research gap by investigating the influence of rotary inertia of the blades and the rotor eccentricity on the nonlinear structural response and failure probabilities of OWTs. Because it has been shown that the OWTs are vulnerable to crustal earthquakes [2,5], a suite of 50 shallow crustal earthquake records is selected for nonlinear dynamic analysis. The changes in the tower damage modes and the seismic fragility [14] of OWTs is then examined using four different combinations of the rotary inertia and the rotor eccentricity. First, M_{RNA} assigned to the tower top while ignoring the rotary inertia of the blades (I_R). Next, the I_R is calculated assuming a uniform distribution of the blade mass (m_B) across the blade length (r_B) as it is applied at the tower top along with M_{RNA} . Third, M_{RNA} and I_R are considered with a vertical eccentricity from the tower top. Fourth, the nacelle (m_N) and the rotor mass (m_R) are considered separately at their center of mass locations, where the I_R is applied at m_R . (i.e., the nacelle and rotor are vertically and horizontally eccentric to the tower top). The modal, non-linear dynamic and fragility analysis results are then discussed to point out the implications of the different pairs of RNA parameters on the high-order vibration modes, tower damage modes and the failure probabilities of OWTs.

2. Structural and load modeling

The monopile-supported NREL 5MW reference OWT is considered as the case study [12,15]. The numerical model of the OWT is developed using the open-source software OpenSees [16]. The main tower, transition piece, and the monopile are modeled by means of non-linear displacement-based elements, which are efficient in capturing the progressing of material non-linearity across the tower [2,5]. Details on the structural specifications, reference axis, and finite element modeling (FEM) of the OWT are shown in Fig. 1(a). The monopile is assumed to embed 36 m into the seabed, which is an elastic homogeneous layer of soil with a unit weight of 10 kN/m³ and internal friction angle of 35°. The soil-pile interaction is modeled considering the monopile as a Winkler beam supported by the API [17] based on non-linear springs (see [2] for more details).

2.1 RNA modeling

The RNA is primarily modeled using the conventional lumped mass approach and it is sub-divided into four-different configurations, referred to as M1 to M4, as shown in Fig. 1(b). M1 considers the total RNA mass (M_{RNA}) at the tower top, where only the effects of the translational masses are considered. M2 to M4 further defines the rotary inertia of the blades (I_R) at the tower top about X, Y, and Z-direction, using the expressions listed in Table 1 [2], where m_B is the blade mass, and r_B is the blade length. It is noted that M1 and M2 do not take into account the eccentricity of the M_{RNA} . M3 considers M_{RNA} located at the rotor shaft at a vertical distance of e_{zS} from the tower top, whereas M4 models the nacelle and the rotor (hub and three blades) separately at a

horizontal and vertical eccentricity of (e_{x_N}, e_{z_N}) and (e_{x_R}, e_{z_R}) from the tower top, respectively. Rigid links are used to achieve a tied kinematic interaction between the tower top and RNA nodes, as shown in Fig. 1(b).

Table 1 – Estimation of I_R for different RNA models

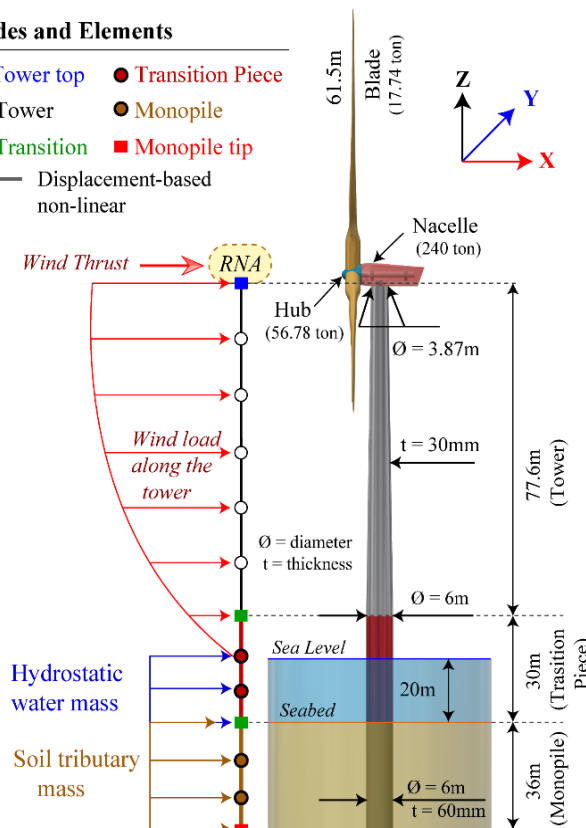
I_R	M1	M2	M3	M4
I_X	0	$m_B r_B^2$		
I_Y	0	$0.5m_B r_B^2 + 3m_B e_{x_R}^2$		$0.5m_B r_B^2$
I_Z	0	$0.5m_B r_B^2 + 3m_B e_{x_R}^2$		$0.5m_B r_B^2$

2.2 Static and dynamic loads

The static loads include the self-weight, hydrostatic effects of the water mass around the tower/transition piece, the soil mass in and around the monopile, and the wind load as shown in Fig. 1(a). The wind loads are applied at the tower and the rotor as nodal loads, whereas the rest of the static loads are considered as the nodal masses. The wind forces at the tower are calculated for normal wind conditions [18] and the wind thrust at the hub is estimated as the function of the rotor swept, formed by the revolution of the blades, following [19]. The seismic loads are considered dynamically and are applied as acceleration time-histories at the monopile springs in all three directions (X, Y, and Z). Due to the limited availability of the geotechnical details, the effects of site amplification and the wave propagation could not be reflected on the input time histories, therefore, the ground motions are uniform at all monopile spring supports.

Nodes and Elements

- Tower top
- Tower
- Transition
- Displacement-based non-linear
- Transition Piece
- Monopile
- Monopile tip



a) Global axis, geometry & FEM description

NREL 5MW

$$\begin{aligned}
 e_{x_N} &= 1.90 \text{ m}, e_{z_N} = 1.75 \text{ m} \\
 e_{x_R} &= -5.00 \text{ m}, e_{z_R} = 2.40 \text{ m} \\
 e_{x_S} &= 0.00 \text{ m}, e_{z_S} = 1.9626 \text{ m}
 \end{aligned}$$

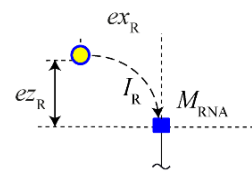
- Tower top
- Rotor shaft
- Hub/Rotor
- ◆ Nacelle
- Tower
- Rigid Link

$$(I_R \rightarrow I_X, I_Y, I_Z) = 0$$

$$M_{RNA}$$

■ RNA mass node
 $M_{RNA} = m_N + m_H + 3m_B$

(i) M1



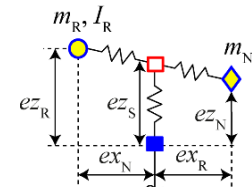
■ RNA mass node
 $I_R \rightarrow \blacksquare$, given e_{x_R}
 where, $e_{z_R} = 0$ (No Eccentricity)

(ii) M2

$$I_R$$

□ RNA mass node
 $I_R \rightarrow \square$, given e_{x_R}
 (Vertical eccentricity = e_{z_S})

(iii) M3



● Rotor mass node
 $m_R = m_H + 3m_B$

(iv) M4

b) RNA (rotor inertia) modeling schemes

Fig. 1 – Schematic representation of the OWT geometry, FEM, and the RNA models

3. Earthquake records

Fig. 3 shows the epicentral locations of the 50 shallow crustal records selected for non-linear time history analysis. The records have a magnitude (M) and source-to-site distance (R) range of 6.4 to 7.8 and 0 to 35 km, respectively. The mean peak ground acceleration (PGA) and peak ground velocity (PGV) is 0.452 g and 68.38 cm/s. The selection criteria are formed on the basis of previous studies that suggested crustal records with $PGV > 30$ cm/s can be detrimental for OWTs [5]. The response spectra of the three components (X, Y, and Z) of the selected records are shown in Fig. 3.

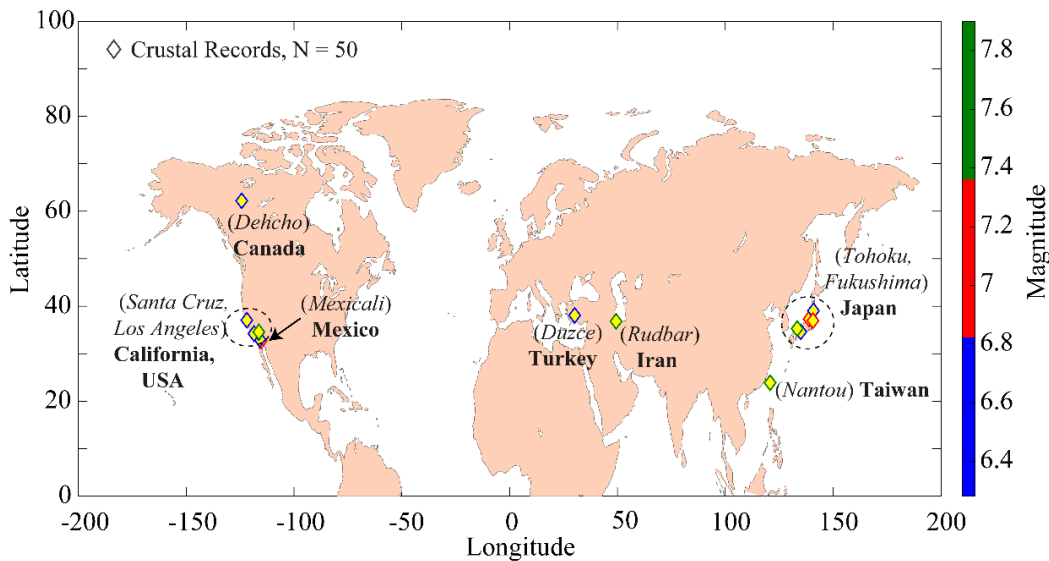


Fig. 2 – Epicentral locations of the shallow crustal records used for time-history analysis

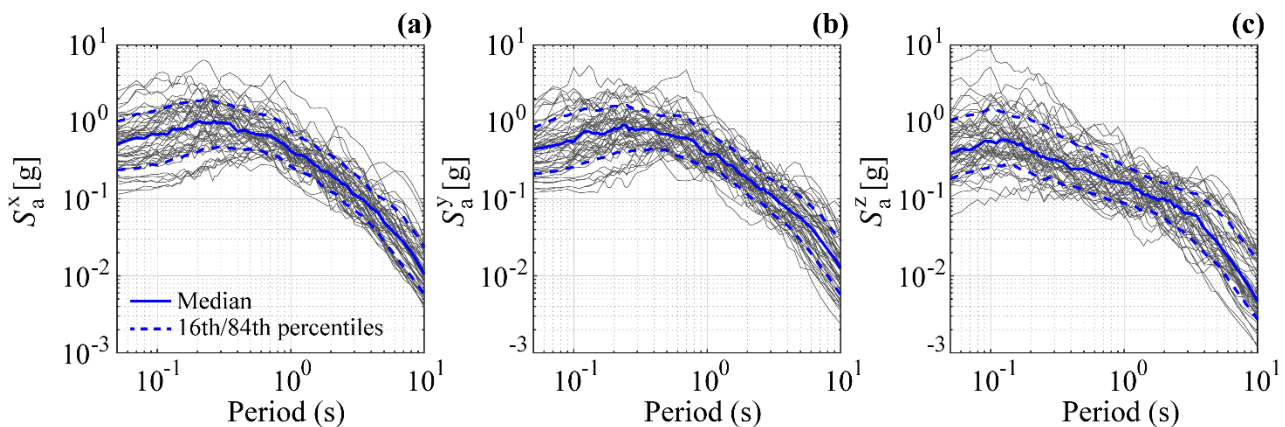


Fig. 3 – Spectral response spectra of the three ground motions components

4. Seismic vulnerability analysis

The influence of rotary inertia and rotor eccentricity on the seismic vulnerability of OWTs is examined using the fragility curves. The fragility function evaluates the conditional probability (p) of an engineering demand parameter (EDP) to exceed a prescribed limit state (LS) at a given earthquake intensity measure (IM) [14]. In this study, the tower's demand-to-capacity ratio (DCR) is adopted as the performance metric (EDP) at both serviceability limit state (SLS) and ultimate limit state (ULS). The demand (D) is obtained as the structural

responses from the non-linear time history analysis and the capacity (C) is prescribed at each LS. The maximum tower top rotation of $\pm 0.5^\circ$ is taken as the SLS, following Det Norske Veritas (DNV) guidelines for monopiles [20]. The strength and stability criteria for thin-walled shells, provided in Annex D of Part 1-6 of the Eurocode 3 is selected for the ULS [21]. Moreover, the first spectral acceleration-averaged over the three ground motion components $S_a^{xyz}(T_1)$ is taken as the potential IM to represent the structural response and the vulnerability for a suite of N earthquake records [5].

The parameters of the fragility model, the EDP , the LS criteria, and the IM ; chosen for this study are expressed in Eq. (1) to (8), which are categorically summarised in Table 2. The terms σ and τ in Eq. (3) and (4) are the meridional and planar shear stress demands on the tower and the foundation, and these are obtained as the structural responses (see [2,21] for more details).

Table 2 – Expressions to estimate the selected EDP at an LS, IM and the fragility function

$(EDP)_{LS}$	$DCR_{SLS} = (\text{Tower top rotation})/0.5^\circ$		(1)
	$DCR_{ULS} = \max \{S_v, S_b\}$		(2)
	Von-Mises stress (σ_{eq}) design check	$S_v = D/C = \sigma_{eq}/f_y = \frac{\sqrt{\sigma^2 + 3\tau^2}}{f_y} \leq 1,$ ($f_y = 355$ MPa)	(3)
	Buckling strength check	$S_b = (\sigma/\sigma_{x,Rd})^{k_x} + (\tau/\tau_{x\theta,Rd})^{k_\tau} \leq 1$	(4)
IM	$S_a^{xyz}(T_1) = [S_a^x(T_1^x) \cdot S_a^y(T_1^y) \cdot S_a^z(T_1^z)]^{1/3}$		(5)
Fragility Model	$p[DCR_{LS} > 1 S_a^{xyz}(T_1)] = \Phi \left[\ln \eta_{DCR_{LS} S_a^{xyz}(T_1)} / \beta_{DCR_{LS} S_a^{xyz}(T_1)} \right]$		(6)
	$\ln \eta_{DCR_{LS} S_a^{xyz}(T_1)} = \ln a + b \ln S_a^{xyz}(T_1)$		(7)
	$\beta_{DCR_{LS} S_a^{xyz}(T_1)} = \sqrt{\sum_{i=1}^N (\ln DCR_{LS,i} - \ln \eta_{DCR_{LS} S_a^{xyz}(T_1)_i})^2 / (N - 2)}$		(8)

5. Results and Discussions

5.1 Modal Analysis

The modal analysis is performed to identify the dynamic characteristics of the OWT with different RNA models (M1 to M4). Fig.4 shows the first four-tower bending mode shapes which are identical for M1 to M4. The difference in their dynamic behavior can be observed by the vibration periods (T) and the participation masses (MP) in the X, Y, and Z-direction, shown in Table 2. In all four cases, there is a uniform distribution of active translational (X, Y) masses among the higher modes. The active masses at each mode (MP_X and MP_Y) tend to reduce when rotary inertia and rotor eccentricity is considered, i.e., M2 to M4. M1 requires 19 modes to achieve approximately 100%, 100%, and 90% mass contribution in X, Y, and Z-direction, whereas for M2 to M4 it takes 22 modes to achieve the same mass. Moreover, the effects of rotary inertia increase the vibration periods, which is more prominent at higher-order (X and Y) modes in M2 to M4, however, there is no effect on the vertical vibrations.

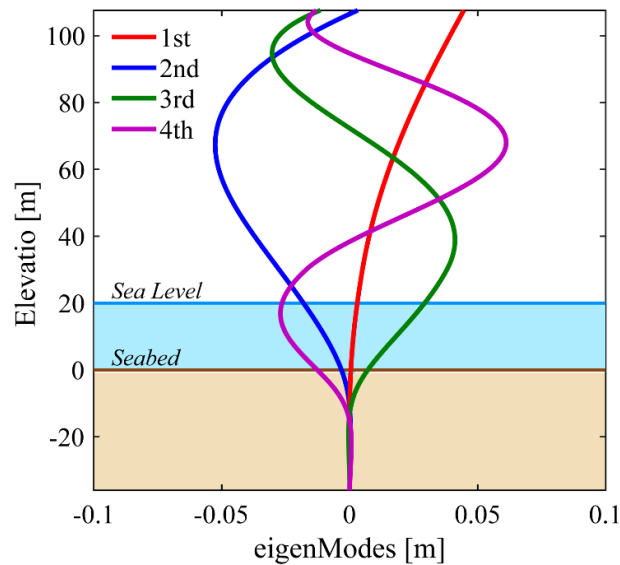


Fig. 4 – First four normalized tower bending mode shapes in the x-direction for M1 to M4

Table 2 – Rotary inertia and eccentricity effects on the modal analysis

Mode	T [sec]				MP _x [%]				MP _y [%]				MP _z [%]			
	M1	M2	M3	M4	M1	M2	M3	M4	M1	M2	M3	M4	M1	M2	M3	M4
1	3.842	3.917	4.016	4.015	-	-	-	-	17.5	16.8	16.6	16.6	-	-	-	-
2	3.842	3.881	3.979	3.981	17.5	17.1	17.0	16.9	-	-	-	-	-	-	-	-
3	0.550	0.759	0.764	0.765	-	-	-	-	10.8	6.3	6.6	6.6	-	-	-	-
4	0.550	0.652	0.664	0.671	10.8	7.9	8.1	7.9	-	-	-	-	-	-	-	-
5	0.224	0.370	0.364	0.364	-	-	-	-	9.2	8.6	8.6	8.6	-	-	-	-
6	0.224	0.328	0.323	0.328	9.2	7.3	7.6	7.6	-	-	-	-	-	-	-	-
7	0.153	0.183	0.181	0.181	-	-	-	-	-	7.7	7.6	7.6	50.1	-	-	-
8	0.115	0.177	0.175	0.176	0.0	7.1	7.0	7.1	6.7	-	-	-	-	-	-	-
9	0.115	0.153	0.153	0.153	6.7	-	-	-	-	-	-	-	-	50.1	50.1	50.0

5.2 Tower stress profiles

The effects of rotary inertia and rotor eccentricity on the tower damage modes are examined on the basis of the tower stresses. Fig. 6 shows the normalized tower stress profiles corresponding to a pair of records that caused the ULS exceedance, which originated in Los Angeles (USA) and Tohoku (Japan). Fig. 6 (a & b) also highlights the key attributes of these records, including the magnitude (M), rupture distance (R), peak ground acceleration (PGA) and the peak ground velocity (PGV). Since the prescribed ULS criterion (Eq. (2)) is driven by the buckling strength of a hollow cylindrical shell, the zones of the tower length, where $DCR_{ULS} > 1$, represent a failure by compression (buckling) [5], which is true for M1 to M4 in Fig. 6 (a & b).

It is noteworthy that the M1 stress profiles are almost identical in Fig. 6 (a & b) and the damage occurs at the same location, i.e., in the middle of the main tower. On the contrary, even though the stress profiles and the damage zones for M2 to M4 are mutually comparable, they differ significantly under the two records. For instance, in the case of Los Angeles, the damage for M2 to M4 occurs in the vicinity of the tower top, whereas, in case of Tohoku, the damage initiates below the mid-tower length and leads up to the top. In addition, the onset of damage appears to shift higher, i.e., towards the slender part of the tower, under the influence of rotary inertia (M2) and the additional rotor eccentricity (M2, M4). Thus, M2 to M4 undergo changes in failure modes as well as their onset locations in comparison to M1, which apart from the absence of rotary inertia can also be attributed to the difference in their high-mode natural frequencies of vibration [6].

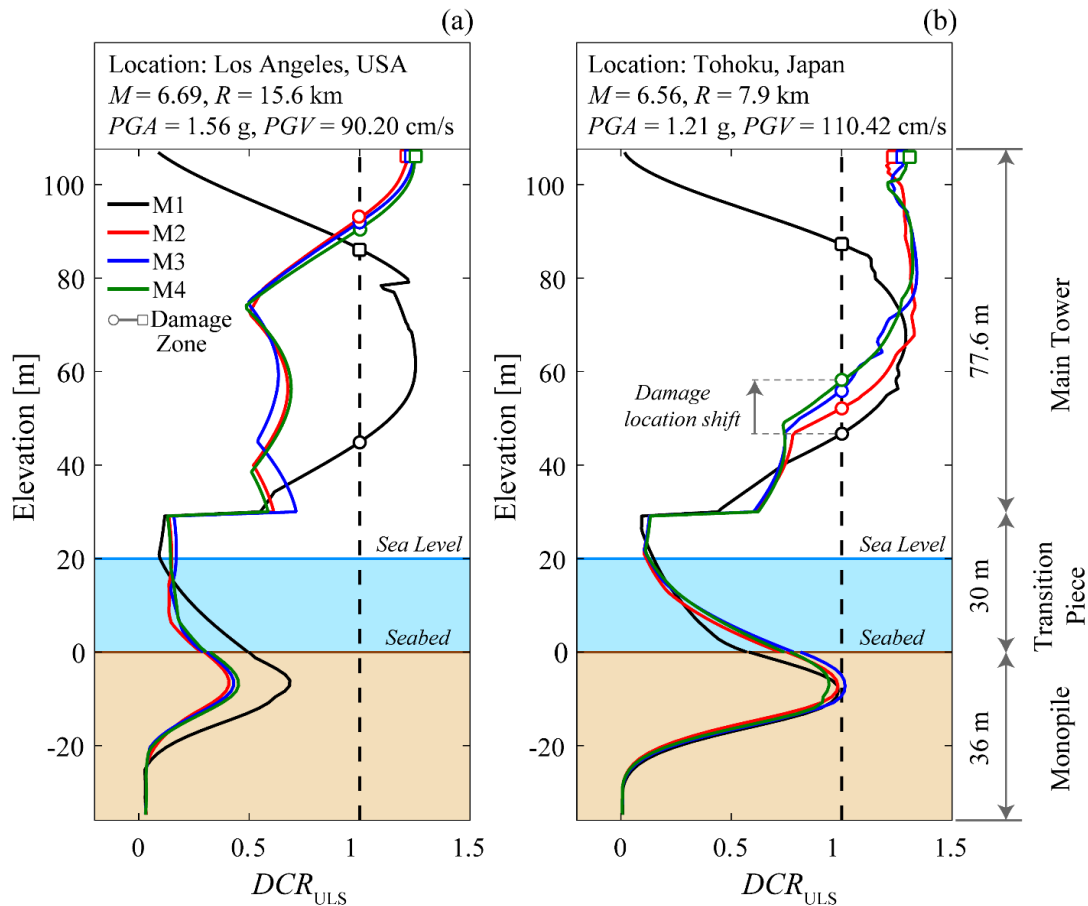


Fig. 6 – Normalized tower stress profiles, showing failure at ULS under crustal records

5.3 Failure probabilities

Fig. 5 shows the probabilities of the DCR exceeding unity, ($p[DCR_{LS}>1]$), at the SLS and ULS. As shown in Fig. 5(a), rotary inertia has a slight-to-negligible influence on the seismic vulnerability of OWTs at the SLS. The fragility curves represent identical, yet high probabilities of reaching the SLS at relatively lower values of $S_a^{xyz}(T_1)$ than the ULS. It is shown in Fig. 5(b) that the seismic vulnerability of OWTs at ULS differs significantly when the rotary inertia is considered. At a given value of $S_a^{xyz}(T_1)$ e.g., 0.75g, $p[DCR_{ULS}>1|0.75g]$ for M1 is 0.58, which increases to 0.75 when rotary inertia is introduced in M2. The value of $p[DCR_{ULS}>1|0.75g]$ further increases to 0.88 due to the influence of the vertical eccentricity (e_{zS}) of the RNA (M3), which remains unaffected by the additional horizontal eccentricity of the nacelle (e_{zN}) and the rotor (e_{zR}) in M4.

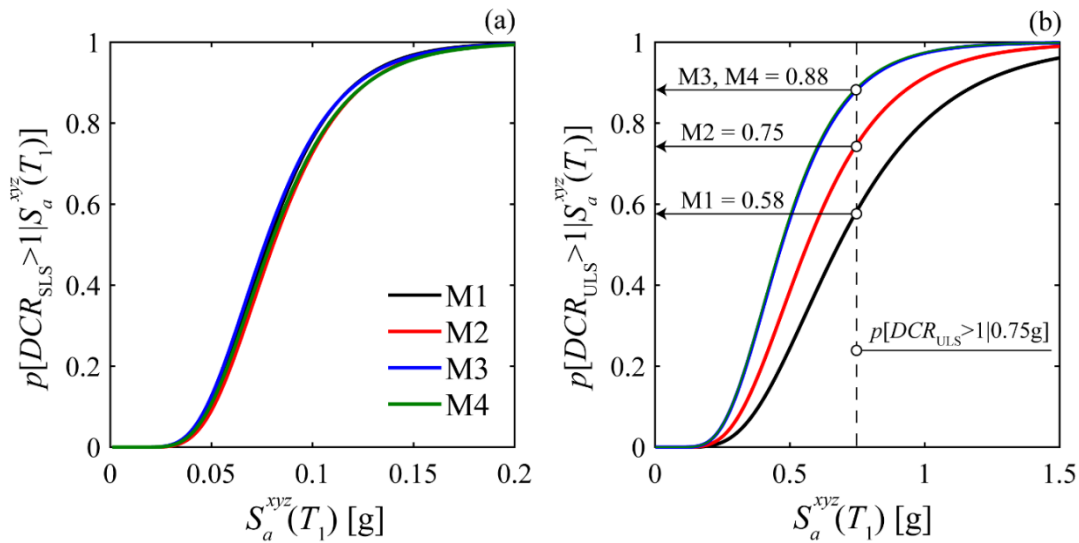


Fig. 5 – Influence of the rotary inertia on the failure probabilities of the 5MW OWT

6. Conclusions and suggestions

The conventional lumped mass approach is generally used to represent the rotor-nacelle-assembly (RNA) in the non-linear dynamic analysis of wind turbines. The present study discusses that the effects of rotary inertia of the blades and eccentricity of the RNA mass are often overlooked and this exclusion can impact the structural response because the RNA contributes significantly to the global mass of the total system. The study also investigates the influence of the rotary inertia and the rotor eccentricity on the damage and failure probabilities of offshore wind turbines (OWT) tower under shallow crustal earthquakes. The conclusions drawn are as follows:

1. The rotary inertia due to blades and the RNA mass eccentricity elongates the vibration periods of the OWT in comparison to the OWT model where the two parameters are neglected (i.e., simplified model M1). The difference is more prominent for the high-order tower bending modes.
2. Conventional model M1 leads to a single damage mode, around the middle of the main tower. On the other hand, when the rotary inertia (M2) and the vertical (M3) and the additional horizontal (M4) eccentricity of the RNA are considered the OWT damage can be localized at two different locations. Failure can occur either near the tower top or start from the middle leading up to the top.
3. The inclusion of the rotary inertia tends to shift the onset of damage to the slenderer section, i.e., the upper part of the tower, and it can move further upwards if the rotor eccentricity is introduced. This can be crucial for the design evaluations of the OWT towers in areas susceptible to shallow crustal earthquakes.
4. The consideration of rotary inertia and the rotor eccentricity has a negligible effect on the allowable tower top deformations. However, at the ultimate limit state (ULS), the OWT that considers the rotary inertia with eccentric RNA (M3, M4) shows the highest probability of the tower failure, which is considerably lower compared to the one predicted when the combined effect of these two parameters is ignored.

In closing, lack of accurate consideration of blades and the RNA mass eccentricity, may lead to prediction of damages modes at different locations while the seismic vulnerability of the OWTs as a whole can be underestimated, at least in areas of shallow crustal earthquake. Furthermore, the lumped mass approach doesn't consider the deformability of the actual blades, which may then affect the structural response due to the presence of the local blade modes, if considered. This also limits the consideration of the structural damping associated with the blade modes in the transient response history analysis. Thus, a refined study is needed to capture a more realistic understanding of the structural behavior and the seismic vulnerability of OWTs.



References

- [1] Prowell I, Veletzos M, Elgamal A, Restrepo J (2009): Experimental and numerical seismic response of a 65 kW wind turbine. *Journal of Earthquake Engineering*, **13** (8), 1172–1190.
- [2] De Risi R, Bhattacharya S, Goda K (2018): Seismic performance assessment of monopile-supported offshore wind turbines using unscaled natural earthquake records. *Soil Dynamics and Earthquake Engineering*, **109**, 154–172.
- [3] Alati N, Failla G, Arena F (2015): Seismic analysis of offshore wind turbines on bottom-fixed support structures. *Phil Trans R Soc A*, **373** (2035), 20140086.
- [4] Ma H, Yang J, Chen L (2017): Numerical analysis of the long-term performance of offshore wind turbines supported by monopiles. *Ocean Engineering*, **136** (January), 94–105.
- [5] Ali A, De Risi R, Sextos A, Goda K, Chang Z (2020): Seismic vulnerability of offshore wind turbines to pulse and non-pulse records. *Earthquake Engineering & Structural Dynamics*, **49** (1), 24–50.
- [6] Nuta E, Christopoulos C, Packer JA (2011): Methodology for seismic risk assessment for tubular steel wind turbine towers: application to Canadian seismic environment. *Canadian Journal of Civil Engineering*, **38** (3), 293–304.
- [7] Sadowski AJ, Camara A, Málaga-Chuquitaype C, Dai K (2017): Seismic analysis of a tall metal wind turbine support tower with realistic geometric imperfections. *Earthquake Engineering & Structural Dynamics*, **46** (2), 201–219.
- [8] Zhao Z, Dai K, Camara A, Bitsuamlak G, Sheng C (2019): Wind Turbine Tower Failure Modes under Seismic and Wind Loads. *Journal of Performance of Constructed Facilities*, **33** (2), 04019015.
- [9] De Biasio M (2014): Ground motion intensity measures for seismic probabilistic risk analysis. Civil Engineering. Université de Grenoble.
- [10] Lee TH, Mosalam KM (2006): *Probabilistic Seismic Evaluation of Reinforced Concrete Structural Components and Systems*.
- [11] Patil A, Jung S, Kwon OS (2016): Structural performance of a parked wind turbine tower subjected to strong ground motions. *Engineering Structures*, **120**, 92–102.
- [12] Jonkman J, Butterfield S, Musial W, Scott G (2009): Definition of a 5-MW Reference Wind Turbine for Offshore System Development (February).
- [13] Dai K, Sheng C, Zhao Z, Yi Z, Camara A, Bitsuamlak G (2017): Nonlinear response history analysis and collapse mode study of a wind turbine tower subjected to tropical cyclonic winds. *Wind and Structures*, **25** (1), 79–100.
- [14] Jalayer F, Ebrahimian H, Miano A, Manfredi G, Sezen H (2017): Analytical fragility assessment using unscaled ground motion records. *Earthquake Engineering and Structural Dynamics*, **46** (15), 2639–2663.
- [15] Jonkman J, Musial W (2010): *Offshore code comparison collaboration (OC3) for IEA Wind Task 23 offshore wind technology and deployment*.
- [16] McKenna F (2011): OpenSees: a framework for earthquake engineering simulation. *Computing in Science & Engineering*, **13** (4), 58–66.
- [17] American Petroleum Institute (2007): Recommended Practice for Planning, Designing and Constructing Fixed Offshore Platforms — Working Stress Design. *API Recommended Practice*, **24-WSD** (December 2000), 242.
- [18] IEC 61400-1 (2005): *Wind Turbines-Part 1: Design Requirements*. International Electrotechnical Commission Geneva, Switzerland.
- [19] Arany L, Bhattacharya S, Macdonald J, Hogan SJ (2017): Design of monopiles for offshore wind turbines in 10 steps. *Soil Dynamics and Earthquake Engineering*, **92** (September 2016), 126–152.
- [20] DNV GL (2014): *Design of Offshore Wind Turbine Structures (DNV-OS-J101)*.
- [21] EN 1993-1-6 (2007): Eurocode 3: Design of Steel Structures-Part 1-6: Strength and Stability of Shell Structures.